Renewable Energy 188 (2022) 721–730

Contents lists available at ScienceDirect

Renewable Energy

journal homepage: www.elsevier.com/locate/renene

MoS_2-based nanofluids as heat transfer fluid in parabolic trough collector technology

Paloma Martínez-Merino , Rodrigo Alcántara , Pedro Gómez-Larrán , Iván Carrillo-Berdugo , Javier Navas *

Departamento de Química Física, Facultad de Ciencias, Universidad de Cádiz, E-11510, Puerto Real, Cádiz, Spain

ARTICLE INFO

Article history:
Received 17 November 2021
Received in revised form
28 January 2022
Accepted 16 February 2022
Available online 23 February 2022

Keywords:
Concentrating solar power
Parabolic trough collectors
Heat transfer fluid
Nanofluids
Molybdenum disulphide
Thermal properties

ABSTRACT

Concentrating solar power is becoming one of options for producing energy to replace conventional polluting energy sources. However, improving the efficiency and reducing the cost of technologies based on this type of energy to make it more competitive is still a work in progress. This study proposes replacing the thermal oil used as the heat transfer fluid in the absorber tubes of parabolic trough solar collectors (PTCs) with nanofluids based on spherical molybdenum disulphide nanoparticles with the aim of improving the thermal efficiency of concentrating solar power plants. The colloidal stability of the nanofluids was verified by Ultraviolet–Visible spectroscopy, Zeta potential and Dynamic Light Scattering monitoring. The presence of spherical MoS_2 nanoparticles resulted in an increase of up to 13% in specific isobaric heat and 6% in thermal conductivity compared to thermal oil. Finally, the efficiency of parabolic trough solar collectors was estimated to increase by 5%, which also favours the decrease of pumping power and the elimination of selective coatings on the absorber tube. To our knowledge, this is the first time that MoS_2-based nanofluids are tested as heat transfer fluids in PTCs analysing its implementation in the solar energy application.

1. Introduction

The depletion of fossil fuels and the environmental damage caused by their combustion has encouraged the search for alternative sources of energy. In this sense, concentrating solar power (CSP) is a type of clean and renewable energy capable of supplying the global energy demand. In 2000, CSP plants produced 1 TWh of energy, rising to 11 TWh in 2017 [1]. Following this growing trend, CSP energy production is expected to reach 180 TWh by 2030 [2], and with the right support and technological advances, 11% of electricity produced in 2050 could be generated by CSP plants [2,3]. Currently, there are four types of CSP technologies [4] that depend on the mirror system to concentrate solar energy: parabolic trough collector [5], linear Fresnel reflector [6], central receiver system [7] and parabolic dish [8]. Among these, parabolic trough collectors (PTC) represent 95% of the total technology installed worldwide [9]. Typically, in CSP plants based on parabolic trough collectors, concave mirrors concentrate solar radiation on the receiver tube that is located in the focus [10,11]. The absorber tubes contain a heat transfer fluid which is heated to 400 °C [12] before being pumped through several heat exchangers to produce superheated steam. Finally, the steam is used in a steam turbine generator to produce electricity [13,14]. However, one of the most significant barriers to concentrating solar power plants based on parabolic trough collectors is their high cost compared to conventional power plants. Therefore, several research lines in recent years have studied ways to improve the overall energy efficiency of CSP plants based on parabolic trough collectors and make them more economically competitive in relation to fossil fuel-based energy production [15]. One of the strategies to enhance the thermal performance of PTC systems is to increase the effective thermal conductivity and the isobaric specific heat of the heat transfer fluid. In this regard, several authors have proposed replacing the HTF in the absorber tube with a colloidal suspension of nano-sized particles, typically known as nanofluids [16,17]. The improvements in thermal properties such as thermal conductivity, isobaric specific heat and thermal diffusivity that nanofluids exhibit compared to conventional fluids make them a promising alternative. Chaudhari et al. [18] obtained an increase of about 7% in the thermal efficiency of parabolic trough solar collectors when using TiO_2/water

* Corresponding author.
E-mail address: javier.navas@uca.es (J. Navas).

https://doi.org/10.1016/j.renene.2022.02.069

Nomenclature

BE	Binding Energy (eV)
C_P	Isobaric specific heat ($J \cdot Kg^{-1}\ K^{-1}$)
L	PTC array total length (m)
T	Temperature (K)

Greek symbols

ρ	Density ($kg\ m^{-3}$)
ψ	Efficiency (–)
$\tilde{v}$	Flow rate ($l \cdot s^{-1}$)
Ø	Volume fraction (%)

Subs and superscripts

bf	Base fluid
coll	Collector
exch	Heat exchanger
max	Maximum
nf	Nanofluid
np	Nanoparticle
out	Outlet
sys	system

Abbreviations

3D-MoS_2	Three-dimensional molybdenum disulfide
CSP	Concentrating Solar Power
DLS	Dynamic Light Scattering
HTF	Heat Transfer Fluid
M3-PALS	Phase Analysis Light Scattering
NTU	Number of transfer units
PEG	Polyethylene Glycol
PTC	Parabolic Trough Collector
TEM	Transmission Electron Microscopy
THB	Transient Hot Bridge
TMDSC	Temperature Modulated Differential Scanning Calorimetry
TRX-100	Triton X-100
UV–Vis spectroscopy	Ultraviolet–visible spectroscopy
XRD	X-ray diffraction (XRD)
XPS	X-ray photoelectron spectroscopy

nanofluids for a weight nanoparticle fraction of 0.1%. Similar improvements were found in the aqueous Al_2O_3 and TiO_2 nanofluids investigated by Subramani et al. [19,20]. These authors studied nanofluids of volumetric concentrations between 0.05% and 0.5% under different turbulent flow conditions. The greatest improvements in collector efficiency at 0.2 vol% were 8.5% and 8.66% for Al_2O_3 and TiO_2 nanofluids, respectively. Kasaeian et al. [21] found that the global efficiency of parabolic trough collector enhanced 5–7% when 0.3% MCNT/mineral oil nanofluid is used, instead of pure oil.

Most of the studies in the literature use water as the base fluid instead of the thermal oil typically used in CSP plants based on parabolic trough collectors. However, the base fluid used to prepare the nanofluids in this study was Dowtherm A™ thermal oil, a eutectic mixture of biphenyl (27%) and diphenyl oxide (73%). There is a need to analyse nanofluids based on this thermal fluid, both in its properties and in its possible application in CSP technology, because the possible enhancement of the global efficiency of CSP plants thanks to the use of nanofluids can be an important contribution to the green transition of the future production of electricity. Furthermore, the nanomaterials typically used for preparing nanofluids are metallic, metal oxides or carbon-based nanoparticles, but only little research has been conducted involving advanced nanomaterials with interesting properties. In this regard, MoS_2 nanoparticles could be a good reagent for the preparation of nanofluids due to their high thermal conductivity compared to the base fluid [22,23]. This study focuses on the preparation of nanofluids based on spherical MoS_2 nanoparticles synthesized in our laboratory. The nanomaterial was characterized extensively, and studies were performed into the temporal stability of the nanofluids as well as their rheological and thermal properties. To our knowledge, this is the first time that MoS_2-based nanofluids are tested as heat transfer fluids in PTCs analysing its implementation in the solar energy application.

2. Materials and methods

2.1. Reagents and equipment

For the synthesis of the MoS_2 nanoparticles, the reagents were ammonium molybdate tetrahydrate ($(NH_4)_6Mo_7O_{24} \cdot 4H_2O$, purity 99%, Alfa Aesar©), citric acid ($C_6H_8O_7$, purity ≥99.5%, Sigma-Aldrich©), ammonium sulfide ($(NH_4)_2S$, 20 wt% solution in water, density 0.997 g/cm^3 at 25 °C, Sigma-Aldrich©) and ammonium hydroxide (NH_4OH, 28–30 wt % solution in water, density 0.89 g/cm^3 at 20 °C, Honeywell Fluka™). In the case of nanofluids, Dowtherm A™ was supplied by Dow Chemical Company©. Triton X-100 (TRX-100, $(C_2H_4O)_nC_{14}H_{22}O$, average molecular weight 625 g/mol, density 1.065 g/cm^3 at 20 °C, Panreac Química S.A.©) and Polyethylene Glycol 200 (PEG-200, $H(OCH_2CH_2)_nOH$, density 1.124–1.126 g/cm^3 at 20 °C, average molecular weight 190–210 g/mol, Sigma Aldrich©) were used as surfactants.

Several techniques were used for characterizing the MoS_2 nanoparticles. X-ray photoelectron spectroscopy (XPS) was performed on a Kratos© (Manchester, United Kingdom) Axis UltraDLD spectrometer. X-ray diffraction (XRD) measurements were performed on a Bruker© (Billerica, Massachusetts, United States) diffractometer, D8 Advanced A25 Davinci. Finally, transmission electron microscopy (TEM) using an FEI© (Waltham, Massachusetts, United States) Talos F200X microscope. Also, nanofluids stability and their thermophysical properties were characterized. For the stability analysis, the extinction coefficient versus time was measured in a modular system incorporating a OceanOptics© (Duiven, The Netherlands) DH2000-Bal halogen lamp and an OceanOptics© USB-2000+; and particle size and ζ potential values were registered in a Zetasizer Nano ZS system supplied by Malvern Instruments Ltd© (Malvern, United Kingdom). In addition, A HR 10 rheometer supplied by TA Instruments© (Milford, Massachusetts, United States) was used to study the viscosity of nanofluids; the isobaric specific heat was measured using a differential scanning calorimeter supplied by Netzsch© (Selb, Deutschland), model DSC 214 Polyma. Finally, thermal conductivity was measured by using a transient hot bridge (THB-100) equipment supplied by Linseis© (Selb, Deutschland).

2.2. Synthesis of spherical MoS_2 nanoparticles

In a typical process [24], 1.20 g of ammonium molybdate and 2.52 g of citric acid were dissolved in 60 ml of distilled water. After the complete dissolution of the reactants, approximately 2 ml of ammonium hydroxide was added dropwise until the solution reached a pH of 4. Subsequently, the solution was kept at 90 °C and

3.75 ml of 20 wt% solution of ammonium sulfide in water was added dropwise. The clear solution changed colour to orange and finally to dark brown. A modification of the method of Deorsola et al. [24] consisted of keeping the solution at 4 °C for three days. The purpose of this modification was to decrease the solubility of the product and maximize the mass of the precipitate obtained. The solution was centrifuged at 10000 rpm for 1 h, and the precipitates were washed in distilled water three times and then dried at 80 °C for 24 h. The black product was calcined at 900 °C for 1 h in flowing N_2.

2.3. Preparation of 3D-MoS_2-based nanofluids

The 3D-MoS_2-based nanofluids were prepared by the two-step method, whereby the previously synthesized spherical MoS_2 nanoparticles were dispersed in the base fluid by applying ultrasound. The base fluid was a solution of surfactant in a thermal oil. The thermal oil used in this study, commercially named Dowtherm A™, is a eutectic mixture of 73% diphenyl oxide ($C_{12}H_{10}O$) and 27% biphenyl ($C_{12}H_{10}$), which is used as a heat transfer fluid in parabolic through solar collectors [25,26]. TRX-100 and PEG-200 were the surfactants used to improve the dispersion of the nanomaterial and the stability of the resulting colloidal system. Previous studies [27] have reported a reduction in the ratio of the components of the surface tension of Dowtherm A™ and its approximation towards that of other transition metal dichalcogenides through the addition of these surfactants. Six nanofluids (Table 1), each with a volume of 50 ml, were prepared that differed with regard to the initial concentration of spherical MoS_2 nanoparticles and the surfactant used. A Sonics Vibra Cell VCX 750 sonicator was used to prepare the nanofluids and the temperature was maintained at 293 K by means of a refrigeration system. Sonication was programmed for 2 h, and a pulse time of 2 s *on* and 4 s *off* was established. After the ultrasound treatment, the resulting MoS_2 nanofluids showed a dark coloration. The nanofluids were named according to the concentration of nanoparticles and the surfactant used.

2.4. Characterization of the 3D-MoS_2 nanomaterial and nanofluids

The synthesized 3D-MoS_2 nanomaterial was extensively characterized. To determine its chemical composition and chemical state bonding, XPS measurements using a monochromatic Al Kα radiation, 20 eV pass energy and an accuracy of 0.1 eV. The crystal structure was analysed by XRD. Finally, the size and morphology of the nanostructures were determined by TEM.

In relation to the nanofluids, a detailed study was performed of their temporal stability, rheological and thermal properties. One of the strategies to analyse the temporal stability of the MoS_2-based nanofluids consisted in the monitoring by UV–Vis spectroscopy of the extinction coefficient at the wavelength of 628 nm, where there is a characteristic band of MoS_2 [28,29]. The extinction coefficient measured is qualitatively related to the MoS_2 concentration in the nanofluids. Therefore, changes in the extinction coefficient values are indicative of agglomeration and sedimentation phenomena.

Table 1
Description of the MoS_2 based nanofluids prepared.

Nanofluid label	3D-MoS_2/wt%	Surfactant
$5 \cdot 10^{-3}$ wt% MoS_2_TRX	$5 \cdot 10^{-3}$	0.12 wt% TRX-100
10^{-2} wt% MoS_2_TRX	10^{-2}	
$1.5 \cdot 10^{-2}$ wt% MoS_2_TRX	$1.5 \cdot 10^{-2}$	
$5 \cdot 10^{-3}$ wt% MoS_2_PEG	$5 \cdot 10^{-3}$	0.25 wt% PEG-200
10^{-2} wt% MoS_2_PEG	10^{-2}	
$1.5 \cdot 10^{-2}$ wt% MoS_2_PEG	$1.5 \cdot 10^{-2}$	

Measurements were performed in triplicate for 30 days. In addition, the agglomeration of the nanoparticles was studied by analysing the evolution of the particle size using the dynamic light scattering (DLS) technique. The repulsion between the nanostructures was analysed by phase analysis light scattering (M3-PALS), which provides the ζ potential values.

The density of the HTF and MoS_2 nanofluids were determined by pycnometry. Also, the viscosity in a temperature range between 298 K and 388 K was measured using a concentric cylinder geometry and the shear rate ranged between 1 s^{-1} and 100 s^{-1}. Concerning the thermal properties, the isobaric specific heat of the samples was determined by the temperature-modulated differential scanning calorimetry (TMDSC) technique. The temperature program established for the determination of isobaric specific heat has been reported in previous studies [30]. The thermal conductivity of the HTF and the 3D-MoS_2-based nanofluids was measured in a temperature range between 298 K and 388 K by means of transient hot bridge technique.

3. Results and discussion

3.1. Characterization of MoS_2 spherical nanoparticles and nanofluids

XPS studies were performed to confirm the chemical composition of the synthesized sample by determining the oxidation state and the chemical state bonding of the elements present in the solid. The survey XP spectrum of Fig. 1a shows peaks arising from C, O, Mo and S elements. The signals located at a binding energy (BE) of 284.6 eV and 531.2 eV are assigned to the C 1s and O 1s contributions. These signals are typically attributed to common contaminants in XPS analysis such as adsorbed species with oxygen, such as hydroxyl or carbonates groups, and also to the presence of adventitious C [31]. Fig. 1b shows a doublet for the Mo 3d contribution that corresponds to the Mo $3d_{3/2}$ at a BE of about 232.8 eV and the Mo $3d_{5/2}$ at a BE of about 229.5 eV. According to the literature [32,33], these BEs for the Mo 3d contributions are associated with the presence of Mo^{4+}, which corroborates the formation of MoS_2. The peak of S 2s [24] was also detected at 226.8 eV in Fig. 1b. The high resolution XP spectrum of the S 2p orbital (Fig. 1c) shows two peaks at 163.7 eV and 162.4 eV that correspond to the S $2p_{1/2}$ and S $2p_{3/2}$ signals [32,33]. These signals are consistent with the presence of S^{2-}, which again confirms the formation of MoS_2. Further evidence of the formation of MoS_2 is the ratio of the atomic concentration S/Mo = 2 obtained from the signals S 2p and Mo 3d.

Fig. 2 shows the XRD pattern of the synthesized powder. Five diffraction peaks were recorded at 14.17°, 32.91°, 39.91°, 50.08° and 58.75°. According to the diffraction pattern in JCPDS card 37–1492, these peaks are related to the (002), (101), (103), (006) and (110) planes, corresponding to the hexagonal structure of MoS_2 with a P63/mmc space group. Therefore, the presence of MoS_2 in the samples synthesized is confirmed by XRD.

The morphology and size of the nanostructures were determined by the TEM technique. The microscopy images in Fig. 3 reveal the formation of spherical nanoparticles, no uniform particle size distribution being observed. Nanoparticles were found with sizes between 30 nm and 150 nm, with a predominance of nanoparticles between 100 and 110 nm. Besides, nanoparticle agglomerates of up to 400 nm were detected. Therefore, the XPS and XRD results demonstrate the formation of MoS_2 while the TEM results confirm the formation of spherical nanoparticles, which proves the efficiency of the synthesis process.

As described in the experimental section, spherical MoS_2 nanoparticles were dispersed in different surfactant and HTF solutions to obtain six nanofluids. In the following, the colloidal

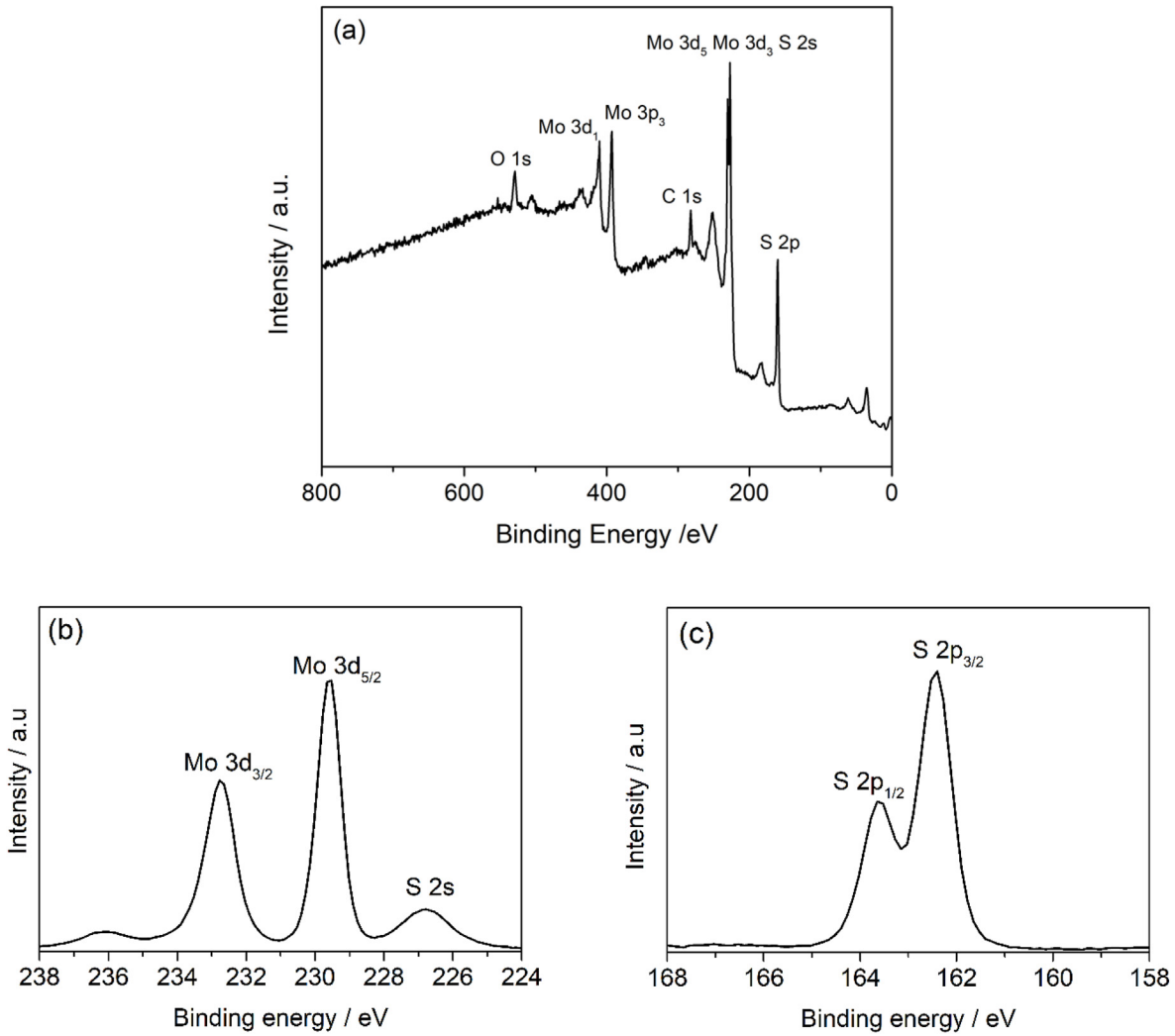

Fig. 1. (a) Survey XP spectrum for synthesized MoS_2 nanoparticles; and high-resolution XP spectra for (b) Mo 3d and (c) S 2p.

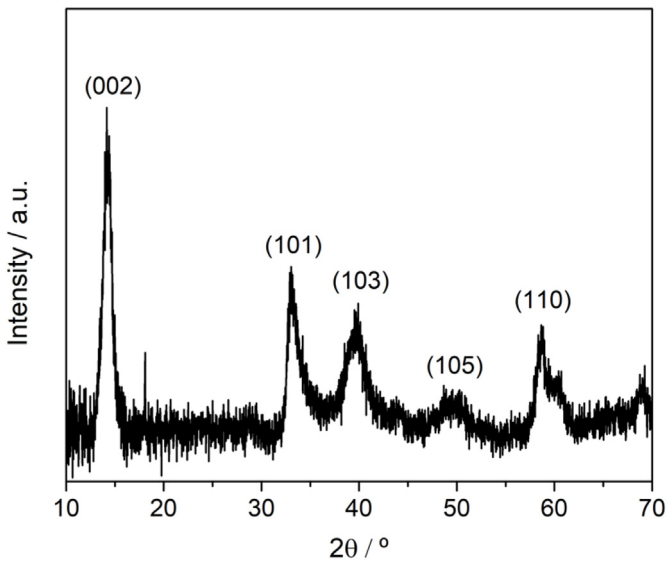

Fig. 2. XRD pattern of the synthesized MoS_2 nanoparticles.

stability and thermal properties of the 3D-MoS_2-based nanofluids will be discussed. The temporal stability of nanofluids plays a key role in their performance since instability can cause pipes to clog and a loss of their thermal enhancements [34,35]. Fig. 4a shows the evolution of the extinction coefficient at 628 nm of the nanofluids over 30 days. The extinction coefficient decreases in all the nanofluids during the first five days. In this period of time, the nanoparticles tend to interact through van der Waals forces and form agglomerates of significant sizes that settle, leading to a decrease in the extinction coefficient of 48–58% in the least concentrated nanofluids and 58–67% in the most concentrated ones. After this initial time period, all the nanofluids, regardless of the nanomaterial concentration, maintained constant extinction coefficient values, which indicates that from the fifth day all the nanofluids were stable. The nanofluids prepared with TRX and with PEG show the same behaviour. Thus, although the more concentrated nanofluids showed a greater decrease in the extinction coefficient, the highest extinction coefficient values were obtained in these nanofluids after 30 days. This means that the amount of MoS_2 nanoparticles dispersed in the fluid is higher in the$1.5 \cdot 10^{-2}$ wt% MoS_2_TRX and $1.5 \cdot 10^{-2}$ wt% MoS_2_PEG nanofluids compared to the rest of the prepared nanofluids. Therefore, these nanofluids are

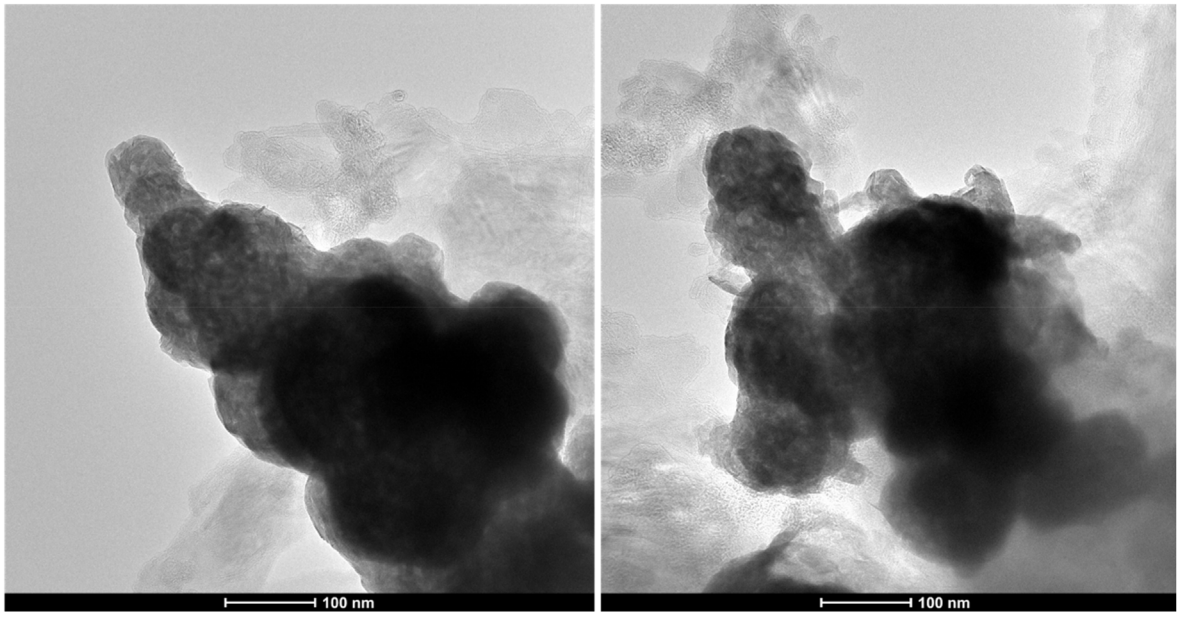

Fig. 3. TEM images obtained for the synthesized MoS_2 nanoparticles.

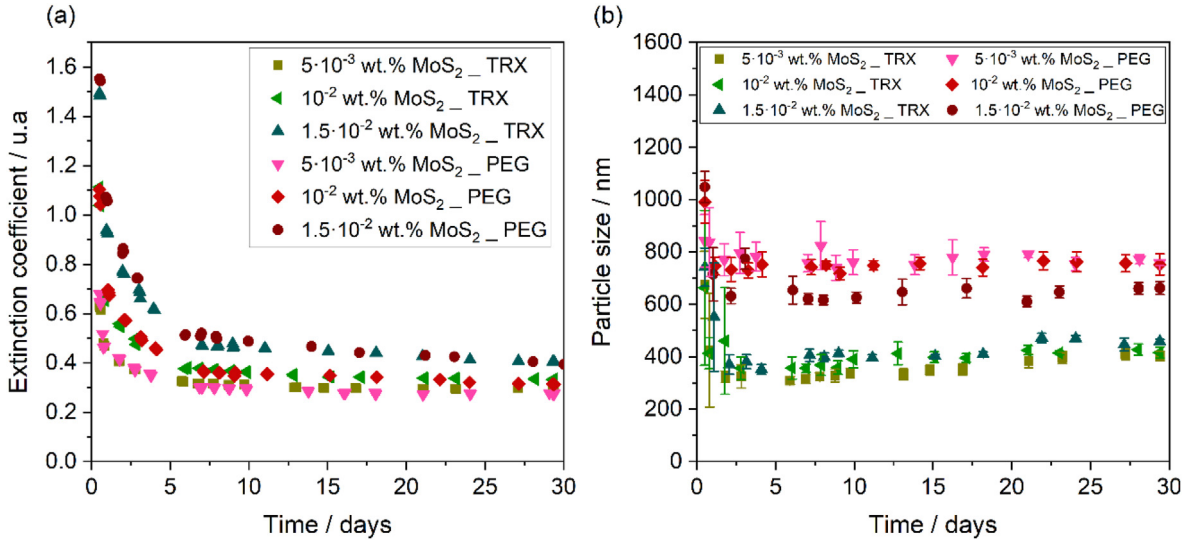

Fig. 4. Evolution over time of the extinction coefficient for MoS_2 nanofluids at $\lambda = 628$ nm (a) and of particle size (b).

expected to present greater thermal improvements.

The UV–Vis results are consistent with the particle size characterization performed by DLS. Fig. 4b shows a higher variability in the first few days when agglomeration and sedimentation processes are more likely. The concentration of MoS_2 nanoparticles is observed not to be an influential factor on the particle size, and neither is the surfactant used. The nanofluids prepared with TRX present an average size of around 350–400 nm while those prepared with PEG exhibit an average size of around 650–800 nm. The longer chain length of TRX compared to PEG may cause a higher steric hindrance on the surface of the MoS_2 nanoparticle, preventing the formation of large agglomerates, which justifies lower particle sizes values than those detected in the nanofluids with PEG.

As in the particle size and UV–Vis results, the ζ potential characterization (Fig. 5) reveals a higher variability in the system during the first few days, after which a constant ζ potential trend is observed for all the nanofluids. The average ζ potential values were around −60 and −80 mV for all the nanofluids, regardless of the concentration of MoS_2 nanoparticles and surfactant used. Typically, ζ potential values between ±40 and ± 60 mV are indicative of good colloidal stability of the nanofluids [36,37]. If the values are greater than ±60 mV, nanofluids are considered to have excellent stability [38]. In the case of the MoS_2 nanofluids in this study, the high ζ potential values measured are evidence of their high stability.

In addition to colloidal stability, other properties of fluids such as density, viscosity, isobaric specific heat and thermal conductivity have a strong influence on heat transfer processes [39,40]. Table 2 shows the density values obtained for the HTF and for the nanofluids by pycnometry at 298 K. These measurements were performed in quintuplicate. It is observed that the presence of nanoparticles increases the density of the base fluid since all the

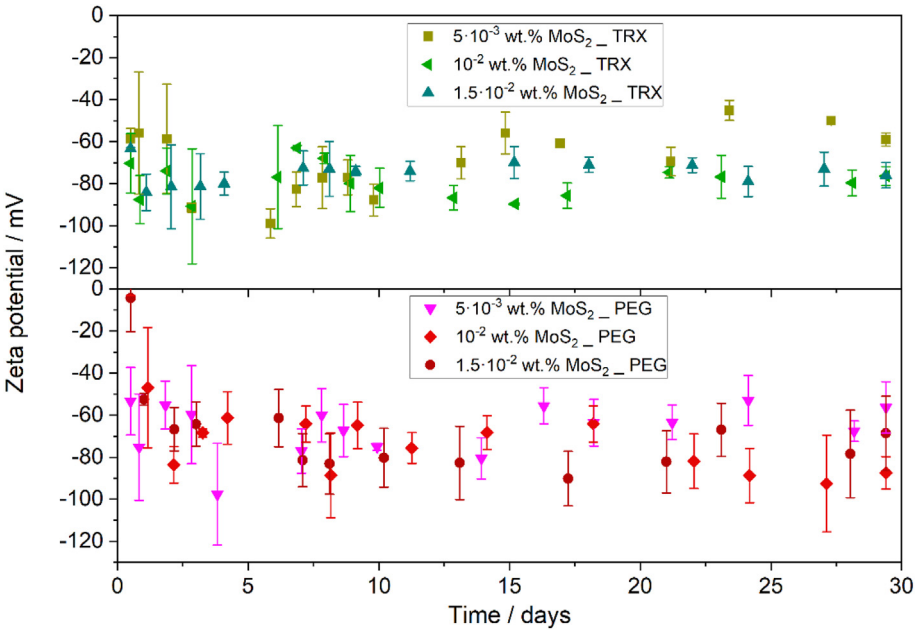

Fig. 5. Evolution over time of the ζ potential values for MoS_2 nanofluids.

MoS_2 nanofluids present higher density values than the HTF. Generally, greater density is associated with an increase in the heat transfer coefficient [41]. In the MoS_2 nanofluids prepared in this study, the density increases with the concentration of MoS_2 nanoparticles. The maximum increase is of 0.95% for the $1.5 \cdot 10^{-2}$ wt% MoS_2_TRX and $1.5 \cdot 10^{-2}$ wt% MoS_2_PEG nanofluids. In addition, the volume fraction can be calculated from density values to determine an effective concentration of the nanofluids when the colloidal stability is reached. Volume fraction was estimated according to $\varphi(vol.\%) = 100 \cdot \left[(\rho_{nf} - \rho_{bf}) / (\rho_{np} - \rho_{bf}) \right]$, where the subscripts nf, bf and np refer nanofluid, base fluid and nanoparticles ($\rho_{np} = 5060$ kg m^{-3}), respectively. The values obtained are shown in Table 2.

An increase in the viscosity of the base fluid due to the addition of nanoparticles can be detrimental to heat transfer and cause pressure drops [42,43]. Fig. 6a shows that the HTF and nanofluids have a Newtonian behaviour as the apparent viscosity remains constant with changing shear rates. Furthermore, the measured viscosity value of the HTF was 3.59 mPa s at 299K while the value provided by the supplier was 3.64 mPa s [26]. The difference between the experimental and supplied value is 1.42%, which demonstrates the accuracy of the experimental method for measuring viscosity. Fig. 6b shows that the viscosity of all the nanofluids and the base fluid decreased with temperature and that the viscosity of the HTF increased slightly with higher concentrations of MoS_2 nanoparticles in the nanofluids. The increases in viscosity are in the range between 0.1 and 4%, with the highest values for the most concentrated nanofluid. Therefore, the use of MoS_2-based nanofluids is not expected to have a negative impact on thermal performance or operational conditions due to the low viscosity increases.

Table 2
Density results obtained for the HTF and MoS_2 nanofluids at 298 K.

Sample	Density/kg · m^{-3}	φ/vol%
HTF	1055.7 ± 0.1	–
$5 \cdot 10^{-3}$ wt% MoS_2_TRX	1062.6 ± 0.1	0.172
10^{-2} wt% MoS_2_TRX	1064.4 ± 0.2	0.217
$1.5 \cdot 10^{-2}$ wt% MoS_2_TRX	1065.4 ± 0.1	0.242
$5 \cdot 10^{-3}$ wt% MoS_2_PEG	1063.7 ± 0.2	0.200
10^{-2} wt% MoS_2_PEG	1064.9 ± 0.2	0.230
$1.5 \cdot 10^{-2}$ wt% MoS_2_PEG	1065.7 ± 0.1	0.250

Regarding the thermal properties of the fluid, Fig. 7a and b shows the isobaric specific heat and thermal conductivity measurements of the nanofluids and HTF. The isobaric specific heat of the MoS_2 nanofluids (see Fig. 7a) followed the same increasing trend with temperature as the HTF. In the case of the HTF, the experimental value only differs by 0.2% from the value provided by the supplier [26]. Note that the isobaric specific heat is higher in the nanofluids than in the HTF, evidence that this value increases due to the presence of MoS_2 nanoparticles. According to the literature, solids typically present lower isobaric specific heat values than liquids, so nanofluids are expected to have lower values than the corresponding base fluid [44]. In this study, the opposite effect occurs, i.e. the MoS_2-based nanofluids had a higher specific isobaric heat than the base fluid, with the difference becoming more significant with increasing temperature. However, this trend has been observed before [45,46] and can be explained if nanofluids are not considered to be a simple mixture of a solid in a liquid. The literature suggests that three main factors are responsible for this behaviour: the energy produced on the surface of the nanoparticles, the interactions between the nanoparticles and the base fluid, and the order of the liquid molecules around the nanoparticle leading to the formation of a semi-solid layer, as has been reported in different systems such Pd-based nanofluids in a thermal oil [47], silica-based nanofluids in molten salts [48], alumina nanofluids using liquid aluminium as the base fluid [49], or in nanofluids modelled by Molecular Dynamics [50]. The present study reports a maximum increase in the isobaric specific heat of up to 13% with respect to the HTF in the 10^{-2} wt% MoS_2_TRX nanofluid at 388 K. These results are favourable considering the beneficial influence of the increase in the isobaric specific heat on the heat transfer enhancement [44].

In addition, the trend of the isobaric specific heat with respect to the nanoparticle concentration (i.e. volume fraction) differs according to the surfactant used. Fig. 7b shows the isobaric specific heat values versus the volume fraction for several temperature

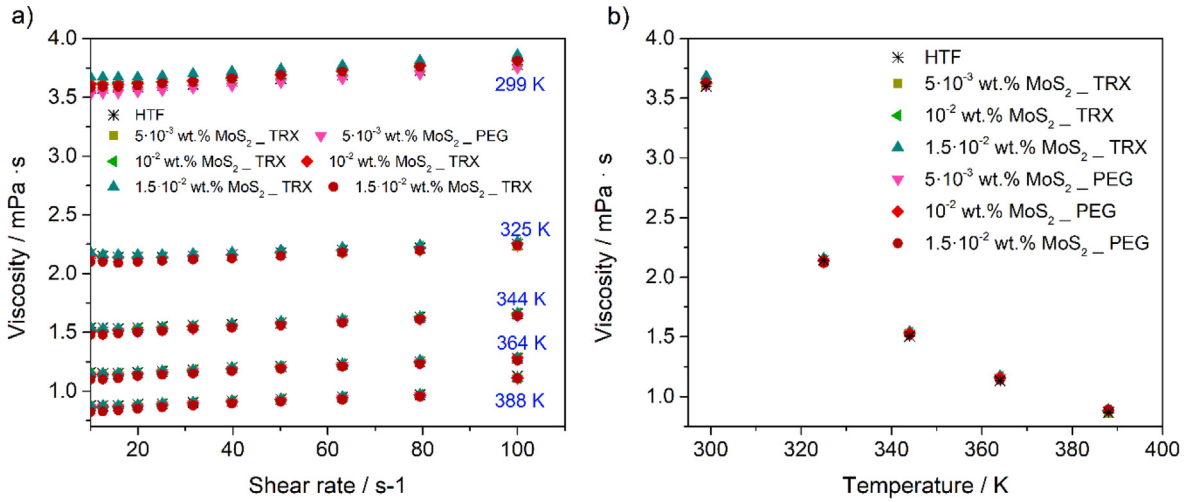

Fig. 6. (a) Viscosity values of HTF and MoS_2 nanofluids at different shear flow rates and at different temperatures, and (b) viscosity of the samples versus temperature at a constant shear flow rate of 25 s^{-1}..

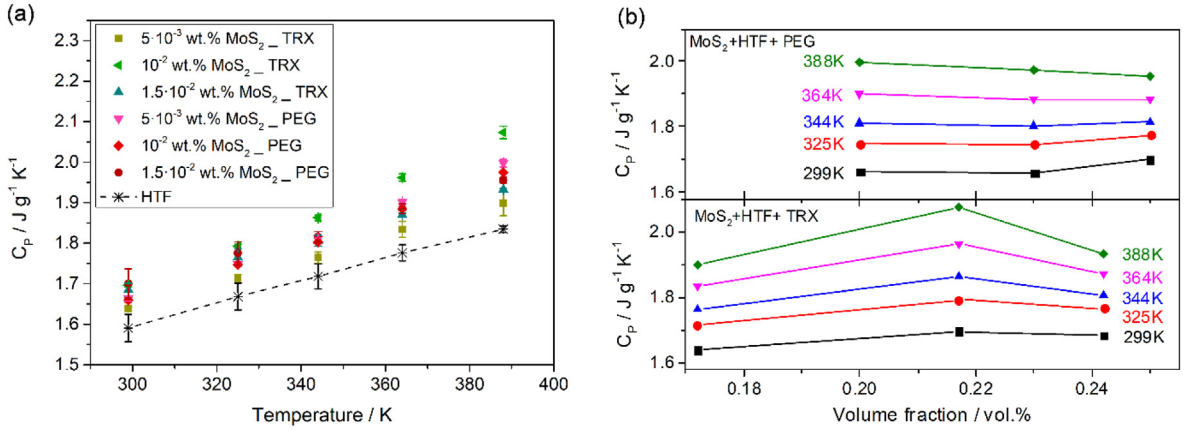

Fig. 7. (a) Isobaric specific heat of MoS_2-based nanofluids versus temperature and (b) volume fraction. At the top of Figure b, the conductivity values of nanofluids prepared with PEG and with a MoS_2 volume fraction of 0.172 vol%, 0.217 vol% and 0.242 vol% are plotted at different temperatures. At the bottom of Figure b, the same analysis has been performed for the nanofluids prepared with Triton X and with a MoS_2 volume fraction of 0.200 vol%, 0.230 vol% and 0.250 vol%.

values. In the case of the nanofluids prepared using PEG, the variation with the volume fraction is slight and for several temperature an increase of isobaric specific heat with the volume fraction is observed. In the case of the nanofluids prepared using TRX-100 as the surfactant, however, the highest values are found at the intermediate concentration. This behaviour cannot be explained by the typical models considering a binary system, but the presence of a solid-liquid interface can explain these values, as reported by Hentschke [51]. According to this model, the increase in the isobaric specific heat up to intermediate concentrations followed by a decrease at higher concentrations may be due to adjacent layers around the nanoparticles overlapping [51]. This means that the internal organization of the components of the nanofluids is different according to the surfactant used, as is observed for the different behaviour of the isobaric specific heat values.

Thermal conductivity is one of the most important properties involved in heat transfer processes of fluids [52,53]. Fig. 8 shows that it increases with temperature in the HTF and nanofluids, which is evidence that the presence of MoS_2 nanoparticles does not alter the trend of the thermal conductivity of the fluid with temperature. It is also noticeable that the enhancements in the thermal

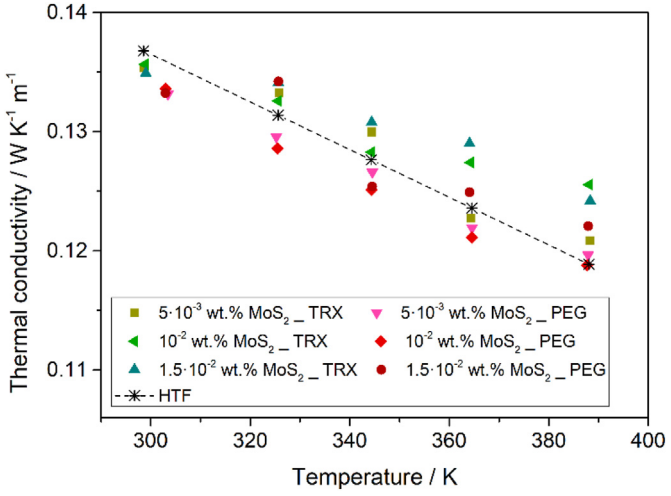

Fig. 8. Evolution of the thermal conductivity values of HTF and MoS_2-based nanofluids with temperature.

conductivity of the MoS_2 nanofluids compared to the HTF becomes more significant at higher temperatures, which is of great interest for their application in parabolic trough collectors, which operate at high temperatures. The highest thermal conductivity values were associated with the nanofluids 10^{-2} wt% MoS_2_TRX and $1.5 \cdot 10^{-2}$ wt% MoS_2_TRX, which exhibited a thermal conductivity enhancement of around 6%. In the case of the nanofluids prepared with PEG, the maximum improvement was of 2% for the $1.5 \cdot 10^{-2}$ wt% MoS_2_PEG. In addition, the less concentrated nanofluids (10^{-2} wt% MoS_2_TRX and 10^{-2} wt% MoS_2_PEG) were the ones with the lowest thermal conductivity for both the TRX-100 and PEG systems. Therefore, the thermal conductivity of the system increases with an increasing concentration of MoS_2 nanoparticles, since the nanofluids of intermediate and higher concentrations had the highest thermal conductivity values regardless of the surfactant used. Furthermore, it is noteworthy that, according to the increasing trend of the thermal conductivity improvements of the nanofluids with temperature, increases of more than 6% could be achieved at a temperature above 388 K. These results are of great interest considering that the heat transfer fluid reaches a temperature close to 673 K in concentrating solar power plants [54].

3.2. Efficiency of nanofluids in solar power plants

In this section, the use of 3D-MoS_2-based nanofluids in concentrating solar power plants has been analysed. The efficiency of the solar collector and the heat exchanger using nanofluids has been compared with the base fluid, which is the typical HTF used in CSP plants using parabolic trough collector technology. To analyse the overall efficiency, the solar collector efficiency and also the effectiveness of the coupled heat exchangers were estimated.

According to the solar collector efficiency, the expected outlet temperature under turbulent flow conditions has been estimated for surface PTCs, used in CSP-PTC plants, and also for volumetric PTCs, which are able to be implemented for dark coloured nanofluids, such as those developed in this study. Two approximate analytic solutions reported by Bellos et al. [55] and O'Keeffe et al. were used [56]. A detailed description of these solutions is included in the Supplementary Material. The mean deviation in the outlet temperature is found to be 0.06% and in the thermal efficiency, 1.16% [55]. Expressions for the outlet temperature, the collector efficiency, the exchanger effectiveness, and the whole efficiency are given in the Supplementary Material for surface and volumetric PTCs. The values of all the variables used in the calculation are shown in the Supplementary Material. The outlet temperature (T_{out}) for both types of collectors, using the base fluid or the nanofluid, is given by the maximum temperature (T_{max}) at which the base fluid is stable, which is 673 K. Thus, for $T_{out} = T_{max}$, the required length for the collectors array (L) to reach 673 K has been estimated. The base fluid with that nanofluid showing the most promising thermal properties were compared, namely the nanofluid prepared using Triton X as surfactant and a MoS_2 concentration of 10^{-2} wt%. For typical surface PTCs, the flow rate ($\tilde{v}$) used was 2.6 l s^{-1}. The value of the flow rate is important in the surface collectors because it should be high enough to maintain the turbulent flow, thus preventing local overheating and thermal stress in the receiver. Moreover, energy losses by radiative processes are minimised. As Fig. 9 shows, for surface PTCs, T_{out} = 673 K for the base fluid at L = 257 m, and at L = 310 m for the nanofluid. In the case of a volumetric collector using the nanofluid with the same geometry and flow rate, T_{out} = 673 K at L = 327 m. Meanwhile, using the base fluid in a volumetric collector is unfeasible due to the pale colour of the fluid. In other words, a volumetric PTC with the same configuration as a surface PTC is less efficient. However, since overheating problems do not apply in volumetric collectors, the flow rate can be decreased. The energy storage capability of the fluid and the nanofluids, given by the product ($\rho \cdot C_P$), is 1928 and 2326 kJ m^{-3} K^{-1} for the base fluid and the nanofluid, respectively. Therefore, it is possible to reduce the flow rate by 20% without affecting the energy storage capability. Thus, the efficiency of volumetric collectors was estimated for a flow rate of 2.0 l s^{-1}. For volumetric PTCs, using the nanofluid prepared in this work, T_{out} = 673 K at L = 261 m. This length is only 4 m greater than that estimated for surface PTCs using the base fluid, which is the standard condition, but volumetric collectors are built without a coating, avoiding higher costs and thermal stress on the surface. The length is greater because the specific heat of the nanofluid is higher, and it needs to be heated to 673 K. However, this does not necessarily imply that using a nanofluid is less efficient because it is necessary to take into account the thermal efficiency of the collector and the effectiveness of the heat exchanger.

The thermal efficiency of the collector, ψ_{coll}, can also be estimated from the solutions of Bellos et al. and O'Keeffe et al., while the heat exchanger effectiveness, ψ_{exch}, was calculated by using the NTU (number of transfer units) method [57]. The complete system efficiency is then given by $\psi_{sys} = \psi_{coll} \cdot \psi_{exch}$. The details of the

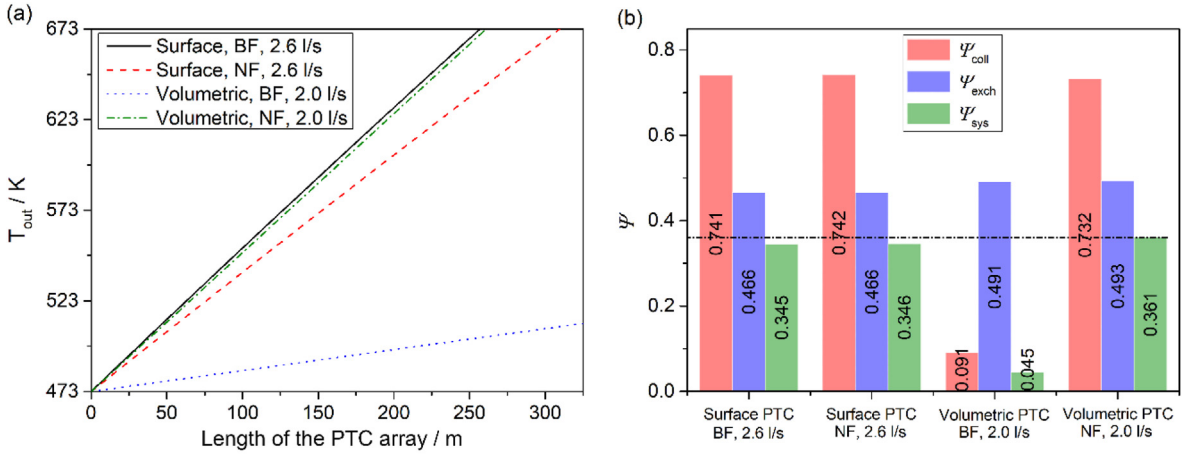

Fig. 9. (a) Outlet temperature in surface and volumetric PTCs using the base fluid (BF) used in this study, which is the typical HTF used in CSP-PTC plants, and the most promising nanofluid (NF) prepared in function of the length of the collectors array; and (b) collector efficiency, effectiveness of the heat exchanger and the overall efficiency for the same configurations.

calculations are shown in the Supplementary Material. Four systems were analysed: (a) surface PTC using the base fluid (the typical HTF used in CSP-PTC plants) and a flow rate of 2.6 l s^{-1}, (b) surface PTC using the nanofluid prepared and a flow rate of 2.6 l s^{-1}, (c) volumetric PTC using the typical HTF and a reduced flow rate of 2.0 l s^{-1}, and (d) volumetric PTCs using the nanofluid and a reduced flow rate of 2.0 l s^{-1}. The results obtained are shown in Fig. 9b. It shows that using either the typical HTF or the nanofluid the collector efficiency is higher for surface PTC than for the volumetric PTC, but the difference is really slight (about 1.3%). In turn, the collector efficiency is similar for the surface PTC using the typical HTF and the nanofluid. In addition, the effectiveness of the heat exchanger is higher for the volumetric PTC using the nanofluid, ~5.4% higher than that for the surface PTC. Considering both efficiencies, the overall efficiency can be analysed. Accordingly, the estimated overall efficiency is ~5% higher for the volumetric PTC using nanofluids (about 36%) than the typical configuration (surface PTC, flow rate 2.6 l s^{-1}, using the typical HTF).

In summary, the use of the nanofluid in a volumetric PTC showed an improvement in the overall efficiency of the system of ~5%, while also reducing the pumping requirements by 20%, the thermal stress on the surface receiver and the cost of the coating needed for the surface PTC; the PTC array was only 1.5% longer (261 m by 257 m, as was described previously). This suggests that nanofluids can help to optimize CSP-PTC plants, and that nanofluids with the right thermophysical properties can increase the overall efficiency of CSP-PTC plants.

4. Conclusions

In the present study, nanofluids based on spherical MoS_2 nanoparticles were prepared and characterised for use as heat transfer fluids in parabolic trough solar collectors. The two-step method was used to prepare 3D-MoS_2-based nanofluids. In the first part step, spherical MoS_2 particles were synthesized by an oxidation-reduction reaction. In the second, the solid was dispersed by ultrasound probe treatment in the eutectic mixture of biphenyl and diphenyl oxide commonly used as the heat transfer fluid in solar collectors. Polyethylene glycol and Triton X proved to be good surfactants for the preparation of these nanofluids since all the nanofluids showed high colloidal stability for about one month. The viscosity of the base fluid was not significantly altered by the presence of MoS_2 nanoparticles in any nanofluid, which avoids problems in heat transfer or pressure drop. The 3D-MoS_2-based nanofluids exhibited improved thermal properties compared to the thermal fluid, the most significant improvements found at higher temperatures. The concentration of MoS_2 nanoparticles has an influence on the thermal improvements, with the best results obtained for nanofluids of an intermediate and higher nanoparticle concentration. Specifically, compared to the base fluid, the isobaric specific heat was increased by up to 13% and the thermal conductivity by up to 6% for the nanofluid prepared with an intermediate MoS_2 nanoparticle concentration and Triton X. The dark colour of the 3D-MoS_2-based nanofluids allows their implementation in volumetric collectors, which, unlike conventional collectors, do not use a selective coating on the absorber tube. According to the numerical analysis, volumetric collectors using MoS_2 nanofluids would improve the overall efficiency by 5%, in addition to reducing the pumping requirements by 20%, the thermal stress on the surface receiver and the cost of the coating needed for the surface PTC. Therefore, nanofluids based on the spherical MoS_2 nanoparticles in this study lead to improvements in the thermal properties of the conventional thermal fluid and the development of a new PTC configuration that would improve the overall efficiency of concentrating solar power plants.

CRediT authorship contribution statement

Paloma Martínez-Merino: Conceptualization, Methodology, Investigation, Writing – original draft. **Rodrigo Alcántara:** Writing – review & editing, Supervision. **Pedro Gómez-Larrán:** Investigation. **Iván Carrillo-Berdugo:** Formal analysis. **Javier Navas:** Writing – review & editing, Supervision, Project administration, Funding acquisition.

Declaration of competing interest

The authors declare that they have no known competing financial interests or personal relationships that could have appeared to influence the work reported in this paper.

Acknowledgements

We acknowledge *Ministerio de Ciencia, Innovación y Universidades del Gobierno de España* for funding under Grant No. RTI2018-096393-B-I00 and for financial support related to measurements of thermal properties, which were performed using devices acquired under Grant No. UNCA15-CE-2945. Also, this research was funded by 2014–2020 ERDF Operational Programme and by the Department of Economy, Knowledge, Business and University of the Regional Government of Andalusia, grant number FEDER-UCA18-107510.

References

[1] World Energy Outlook 2018, International Energy Agency, Paris, France, 2018.
[2] Concentrating Solar Power, International Energy Agency, Paris, France, 2020.
[3] A. Calderon, C. Barreneche, C. Prieto, M. Segarra, A.I. Fernandez, Concentrating solar power technologies: a bibliometric study of past, present and future trends in concentrating solar power research, Front. Mech. Eng-Switz. 7 (2021) 682592.
[4] O. Behar, A. Khellaf, K. Mohammedi, A review of studies on central receiver solar thermal power plants, Renew. Sustain. Energy Rev. 23 (2013) 12–39.
[5] A. Fernandez-Garcia, E. Zarza, L. Valenzuela, M. Perez, Parabolic-trough solar collectors and their applications, Renew. Sustain. Energy Rev. 14 (7) (2010) 1695–1721.
[6] G.D. Zhu, T. Wendelin, M.J. Wagner, C. Kutscher, History, current state, and future of linear Fresnel concentrating solar collectors, Sol. Energy 103 (2014) 639–652.
[7] M.T. Islam, N. Huda, A.B. Abdullah, R. Saidur, A comprehensive review of state-of-the-art concentrating solar power (CSP) technologies: current status and research trends, Renew. Sustain. Energy Rev. 91 (2018) 987–1018.
[8] J. Coventry, C. Andraka, Dish systems for CSP, Sol. Energy 152 (2017) 140–170.
[9] J. Paetzold, S. Cochard, A. Vassallo, D.F. Fletcher, Wind engineering analysis of parabolic trough solar collectors: the effects of varying the trough depth, J. Wind Eng. Ind. Aerod. 135 (2014) 118–128.
[10] D.A. Baharoon, H.A. Rahman, W.Z.W. Omar, S.O. Fadhl, Historical development of concentrating solar power technologies to generate clean electricity efficiently - a review, Renew. Sustain. Energy Rev. 41 (2015) 996–1027.
[11] L.A. Weinstein, J. Loomis, B. Bhatia, D.M. Bierman, E.N. Wang, G. Chen, Concentrating solar power, Chem. Rev. 115 (23) (2015) 12797–12838.
[12] S. Qazi, Solar Thermal Electricity and Solar Insolation, Standalone Photovoltaic (Pv) Systems for Disaster Relief and Remote Areas, 2017, pp. 203–237.
[13] M.T. Dunham, B.D. Iverson, High-efficiency thermodynamic power cycles for concentrated solar power systems, Renew. Sustain. Energy Rev. 30 (2014) 758–770.
[14] M. Romero, J. Gonzalez-Aguilar, Solar thermal CSP technology, Wires Energy Environ. 3 (1) (2014) 42–59.
[15] M. Liu, N.H.S. Tay, S. Bell, M. Belusko, R. Jacob, G. Will, W. Saman, F. Bruno, Review on concentrating solar power plants and new developments in high temperature thermal energy storage technologies, Renew. Sustain. Energy Rev. 53 (2016) 1411–1432.
[16] E. Bellos, Z. Said, C. Tzivanidis, The use of nanofluids in solar concentrating technologies: a comprehensive review, J. Clean. Prod. 196 (2018) 84–99.
[17] U. Srivastva, R.K. Malhotra, S.C. Kaushik, Review of heat transport properties of solar heat transfer fluids, J. Therm. Anal. Calorim. 130 (2) (2017) 605–621.
[18] K.S. Chaudhari, P.V. Walke, U.S. Wankhede, R.S. Shelke, An experimental investigation of a nanofluid (Al2O3+H2O) based parabolic trough solar collectors, Br. J. Appl. Sci. Technol. 9 (6) (2015) 551–557.
[19] J. Subramani, P.K. Nagarajan, S. Wongwises, S.A. El-Agouz, R. Sathyamurthy, Experimental study on the thermal performance and heat transfer characteristics of solar parabolic trough collector using Al2O3 nanofluids, Environ.

Prog. Sustain. 37 (3) (2018) 1149–1159.
[20] J. Subramani, P.K. Nagarajan, O. Mahian, R. Sathyamurthy, Efficiency and heat transfer improvements in a parabolic trough solar collector using TiO2 nanofluids under turbulent flow regime, Renew. Energy 119 (2018) 19–31.
[21] A. Kasaeian, S. Daviran, R.D. Azarian, A. Rashidi, Performance evaluation and nanofluid using capability study of a solar parabolic trough collector, Energy Convers. Manag. 89 (2015) 368–375.
[22] B. Peng, H. Zhang, H.Z. Shao, Y.C. Xu, X.C. Zhang, H.Y. Zhu, Thermal conductivity of monolayer MoS2, MoSe2, and WS2: interplay of mass effect, interatomic bonding and anharmonicity, RSC Adv. 6 (7) (2016) 5767–5773.
[23] Y.X. Wang, N. Xu, D.Y. Li, J. Zhu, Thermal properties of two dimensional layered materials, Adv. Funct. Mater. 27 (19) (2017).
[24] F.A. Deorsola, N. Russo, G.A. Blengini, D. Fino, Synthesis, characterization and environmental assessment of nanosized MoS2 particles for lubricants applications, Chem. Eng. J. 195 (2012) 1–6.
[25] K. Vignarooban, X.H. Xu, A. Arvay, K. Hsu, A.M. Kannan, Heat transfer fluids for concentrating solar power systems - a review, Appl. Energy 146 (2015) 383–396.
[26] Heat Transfer Fluid. Product Technical Data, VLL0-V0100-MA-001, Company TD. Dowtherm A, 1997.
[27] M. Teruel, T. Aguilar, P. Martinez-Merino, I. Carrillo-Berdugo, J.J. Gallardo-Bernal, R. Gomez-Villarejo, R. Alcantara, C. Fernandez-Lorenzo, J. Navas, 2D MoSe2-based nanofluids prepared by liquid phase exfoliation for heat transfer applications in concentrating solar power, Sol. Energy Mater. Sol. Cell. 200 (2019).
[28] Z.S. Guan, C. Wang, W.J. Li, S.B. Luo, Y.B. Yao, S.H. Yu, R. Sun, C.P. Wong, A facile and clean process for exfoliating MoS2 nanosheets assisted by a surface active agent in aqueous solution, Nanotechnology 29 (42) (2018).
[29] N. Savjani, E.A. Lewis, R.A.D. Pattrick, S.J. Haigh, P. O'Brien, MoS2 nanosheet production by the direct exfoliation of molybdenite minerals from several type-localities, RSC Adv. 4 (67) (2014) 35609–35613.
[30] T. Aguilar, J. Navas, A. Sanchez-Coronilla, E.I. Martin, J.J. Gallardo, P. Martinez-Merino, R. Gomez-Villarejo, J.C. Pinero, R. Alcantara, C. Fernandez-Lorenzo, Investigation of enhanced thermal properties in NiO-based nanofluids for concentrating solar power applications: a molecular dynamics and experimental analysis, Appl. Energy 211 (2018) 677–688.
[31] Y.Y. Peng, Z.Y. Meng, C. Zhong, J. Lu, W.C. Yu, Y.B. Jia, Y.T. Qian, Hydrothermal synthesis and characterization of single-molecular-layer MoS2 and MoSe2, Chem. Lett. 8 (2001) 772–773.
[32] R.F. Zhang, Y. Li, J. Qi, D.Q. Gao, Ferromagnetism in ultrathin MoS2 nanosheets: from amorphous to crystalline, Nanoscale Res. Lett. 9 (2014).
[33] H.A. Pineda-Leon, A. Carrillo-Castillo, R. Ochoa-Landin, M.C. Acosta-Enriquez, G. Gutierrez-Heredia, S.G. Ruvalcaba-Manzo, S.J. Castillo, Synthesis and characterization of molibdenum sulfide nanoparticles by a new chemical reaction formulation, Chalcogenide Lett. 15 (8) (2018) 419–424.
[34] X.L. Wang, L. Luo, J.W. Xiang, S.L. Zheng, S. Shittu, Z.Y. Wang, X.D. Zhao, A comprehensive review on the application of nanofluid in heat pipe based on the machine learning: theory, application and prediction, Renew. Sustain. Energy Rev. 150 (2021).
[35] Babita, S.K. Sharma, S.M. Gupta, Preparation and evaluation of stable nanofluids for heat transfer application: a review, Exp. Therm. Fluid Sci. 79 (2016) 202–212.
[36] S.N.M. Zainon, W.H. Azmi, Recent progress on stability and thermo-physical properties of mono and hybrid towards green nanofluids, Micromach.-Basel 12 (2) (2021).
[37] S. Mukherjee, P.C. Mishra, P. Chaudhuri, Stability of heat transfer nanofluids - a review, Chembio. Rev. 5 (5) (2018) 312–333.
[38] M. Sandhya, D. Ramasamy, K. Sudhakar, K. Kadirgama, W.S.W. Harun, Ultrasonication an intensifying tool for preparation of stable nanofluids and study the time influence on distinct properties of graphene nanofluids - a systematic overview, Ultrason. Sonochem. 73 (2021).
[39] D.K. Devendiran, V.A. Amirtham, A review on preparation, characterization, properties and applications of nanofluids, Renew. Sustain. Energy Rev. 60 (2016) 21–40.
[40] M. Gupta, V. Singh, R. Kumar, Z. Said, A review on thermophysical properties of nanofluids and heat transfer applications, Renew. Sustain. Energy Rev. 74 (2017) 638–670.
[41] E.V. Timofeeva, W.H. Yu, D.M. France, D. Singh, J.L. Routbort, Nanofluids for heat transfer: an engineering approach, Nanoscale Res. Lett. 6 (2011).
[42] K. Bashirnezhad, S. Bazri, M.R. Safaei, M. Goodarzi, M. Dahari, O. Mahian, A.S. Dalkilica, S. Wongwises, Viscosity of nanofluids: a review of recent experimental studies, Int. Commun. Heat. Mass 73 (2016) 114–123.
[43] D.S. Udawattha, M. Narayana, U.P.L. Wijayarathne, Predicting the effective viscosity of nanofluids based on the rheology of suspensions of solid particles, J. King Saud Univ. Sci. 31 (3) (2019) 412–426.
[44] M. Chandrasekar, S. Suresh, T. Senthilkumar, Mechanisms proposed through experimental investigations on thermophysical properties and forced convective heat transfer characteristics of various nanofluids - a review, Renew. Sustain. Energy Rev. 16 (6) (2012) 3917–3938.
[45] R. Gomez-Villarejo, E.I. Martin, A. Sanchez-Coronilla, T. Aguilar, J.J. Gallardo, P. Martinez-Merino, I. Carrillo-Berdugo, R. Alcantara, C. Fernandez-Lorenzo, J. Navas, Towards the improvement of the global efficiency of concentrating solar power plants by using Pt-based nanofluids: the internal molecular structure effect, Appl. Energy 228 (2018) 2262–2274.
[46] P. Martinez-Merino, E. Sani, L. Mercatelli, R. Alcantara, J. Navas, WSe2 nanosheets synthesized by a solvothermal process as advanced nanofluids for thermal solar energy, Acs Sustain. Chem. Eng. 8 (3) (2020) 1627–1636.
[47] I. Carrillo-Berdugo, R. Grau-Crespo, D. Zorrilla, J. Navas, Interfacial molecular layering enhances specific heat of nanofluids: evidence from molecular dynamics, J. Mol. Liq. 325 (2021).
[48] D. Shin, D. Banerjee, Enhancement of specific heat capacity of high-temperature silica-nanofluids synthesized in alkali chloride salt eutectics for solar thermal-energy storage applications, Int. J. Heat Mass Tran. 54 (5–6) (2011) 1064–1070.
[49] S.H. Oh, Y. Kauffmann, C. Scheu, W.D. Kaplan, M. Ruhle, Ordered liquid aluminum at the interface with sapphire, Science 310 (5748) (2005) 661–663.
[50] L. Xue, P. Keblinski, S.R. Phillpot, S.U.S. Choi, J.A. Eastman, Effect of liquid layering at the liquid-solid interface on thermal transport, Int. J. Heat Mass Tran. 47 (19–20) (2004) 4277–4284.
[51] R. Hentschke, On the specific heat capacity enhancement in nanofluids, Nanoscale Res. Lett. 11 (2016).
[52] H.Q. Xie, W. Yu, Y. Li, L.F. Chen, Discussion on the thermal conductivity enhancement of nanofluids, Nanoscale Res. Lett. 6 (2011).
[53] M. Lomascolo, G. Colangelo, M. Milanese, A. de Risi, Review of heat transfer in nanofluids: conductive, convective and radiative experimental results, Renew. Sustain. Energy Rev. 43 (2015) 1182–1198.
[54] Y. Krishna, M. Faizal, R. Saidur, K.C. Ng, N. Aslfattahi, State-of-the-art heat transfer fluids for parabolic trough collector, Int. J. Heat Mass Tran. 152 (2020).
[55] E. Bellos, C. Tzivanidis, Analytical expression of parabolic trough solar collector performance, Designs 2 (9) (2018) 1–17.
[56] G.J. O'Keeffe, S.L. Mitchell, T.G. Myers, V. Cregan, Modelling the efficiency of a nanofluid-based direct absorption parabolic trough solar collector, Sol. Energy 159 (2018) 44–54.
[57] T.L. Bergman, A.S. Lavine, F.P. Incropera, D.P. Dewitt, Fundamentals of Heat and Mass Transfer, seventh ed., John Wiley & Sons, New Jersey, USA, 2011.